Published in final edited form as:

J Invest Dermatol. 2015 December ; 135(12): 3133–3143. doi:10.1038/jid.2015.314.

Increased Susceptibility to Skin Carcinogenesis Associated with a Spontaneous Mouse Mutation in the Palmitoyl Transferase *Zdhhc13* gene

Carlos J. Perez[1], **Lars Mecklenburg**[2], **Jean Jaubert**[3], **Lucia Martinez Santamaria**[4,5,6,7], **Brian M. Iritani**[8], **Alexsandra Espejo**[1], **Eleonora Napoli**[9], **Gyu Song**[9], **Marcela del Río**[4,5,6,7], **John DiGiovanni**[10], **Cecilia Giulivi**[9,11], **Mark T. Bedford**[1,12], **Sharon Y.R. Dent**[1,12], **Richard D. Wood**[1,12], **Donna F. Kusewitt**[1,12], **Jean Louis Guénet**[3], **Claudio J. Conti**[1,4,7], and **Fernando Benavides**[1,12]

[1]Department of Epigenetics and Molecular Carcinogenesis, The University of Texas MD Anderson Cancer Center, Smithville, Texas, USA.

[2]Mecklenburg consulting, Hamburg, Germany.

[3]Unité de Génétique Fonctionnelle de la Souris, Institut Pasteur, Paris, France.

[4]Department of Bioengineering, Universidad Carlos III de Madrid, Madrid, Spain.

[5]Regenerative Medicine Unit, Centro de Investigaciones Energéticas, Medioambientales y Tecnológicas (CIEMAT), Madrid, Spain.

[6]Centre for Biomedical Network Research on Rare Diseases (CIBERER), Madrid, Spain.

[7]Instituto de Investigación Sanitaria de la Fundación Jiménez Díaz (IIS FJD), Madrid, Spain

[8]The Department of Comparative Medicine, University of Washington, Seattle, Washington, USA.

[9]Department of Molecular Biosciences, School of Veterinary Medicine, University of California Davis, Davis, California, USA.

[10]Dell Pediatric Research Institute, University of Texas, Austin, Texas, USA.

[11]Medical Investigations of Neurodevelopmental Disorders (M. I. N. D.) Institute, University of California Davis, Sacramento, California, USA

[12]The University of Texas Graduate School of Biomedical Sciences at Houston, Texas, USA.

Abstract

Here we describe a spontaneous mutation in the *Zdhhc13* (zinc finger, DHHC domain containing 13) gene (also called *Hip14l*), one of 24 genes encoding palmitoyl acyltransferase (PAT) enzymes in the mouse. This mutation (*Zdhhc13*^{luc}) was identified as a nonsense base substitution, which

Correspondence: Dr Fernando Benavides, Department of Epigenetics and Molecular Carcinogenesis, The University of Texas MD Anderson Cancer Center, Smithville, Texas 78957, USA. ; Email: fbenavid@mdanderson.org

The authors state no conflict of interest.

results in a premature stop codon that generates a truncated form of the ZDHHC13 protein, representing a potential loss-of-function allele. Homozygous *Zdhhc13*^{luc}/*Zdhhc13*^{luc} mice developed generalized hypotrichosis, associated with abnormal hair cycle, epidermal and sebaceous gland hyperplasia, hyperkeratosis and increased epidermal thickness. Increased keratinocyte proliferation and accelerated transit from basal to more differentiated layers were observed in mutant compared to wild-type epidermis, in untreated skin and after short-term 12-O-tetradecanoyl-phorbol-13-acetate (TPA) treatment and acute UVB exposure. Interestingly, this epidermal phenotype was associated with constitutive activation of NF-κB (RelA) and increased neutrophil recruitment and elastase activity. Furthermore, tumor multiplicity and malignant progression of papillomas after chemical skin carcinogenesis were significantly higher in mutant mice than wild-type littermates. To our knowledge, this is the first report of a protective role for a PAT in skin carcinogenesis.

INTRODUCTION

Protein palmitoylation is one of the most frequent post-translational modifications and is mediated by palmitoyl acyltransferase (PAT) enzymes, a group of cysteine-rich DHHC domain containing proteins (Fukata *et al.*, 2006; Mitchell *et al.*, 2006; Linder and Deschenes, 2007; Levental *et al.*, 2010). The reversible addition of palmitate to cysteine residues is a dynamic process, unique among lipid modifications (Planey and Zacharias, 2009). Palmitoylation increases the lipophilicity of proteins, influencing their subcellular distribution, trafficking and function (Draper *et al.*, 2007; Linder and Deschenes, 2007). In humans, there are 23 DHHC genes described. In the mouse, there are 24 DHHC genes annotated: *Zdhhc1–Zdhhc25* (*Zdhhc10* is skipped). *Zdhhc13* (zinc finger, DHHC domain containing 13) is a member of the PAT family and is also known as *Hip14l* (Huntingtin-interacting protein 14-like) (Goytain *et al.*, 2008).

In this report we present *luca* (symbol: *luc*), a naturally occurring recessive mutation in the mouse *Zdhhc13* gene (*Zdhhc13*^{luc}). Homozygous *Zdhhc13*^{luc}/*Zdhhc13*^{luc} mice develop generalized hypotrichosis with diffuse alopecia. Increased epidermal cell proliferation was observed in mutant skin relative to wild-type (WT) skin after short-term applications of 12-O-tetradecanoyl-phorbol-13-acetate (TPA) and acute UVB exposure. This exacerbated reaction of the mutant skin was always associated with constitutive activation of the NF-κB signaling pathway and enhanced neutrophilic infiltration of the dermis. We also carried out chemical skin carcinogenesis and found that the multiplicity and malignant progression of papillomas were significantly higher in mutant mice when compared with WT littermates. To our knowledge, this is the first report of a protective role of a PAT in a mouse model of carcinogenesis.

RESULTS

Phenotype of *Zdhhc13*^{luc}/*Zdhhc13*^{luc} mice

Homozygous *Zdhhc13*^{luc}/*Zdhhc13*^{luc} (*luc*/*luc*) mice are distinguished from WT littermates at around postnatal day 5 (P5) by a reduced number of emerging hair shafts (HS) and shorter vibrissae. By P15, mutant mice start to show sparse hair coat (particularly in the head) and

irritated skin, sometimes associated with erythema on the face and extremities (**Figure 1a**). After weaning, mutant mice exhibit generalized hypotrichosis and start displaying a characteristic lack of hair around the eyes (**Figure 1b**). No obvious phenotypic differences were observed in mutant mice among the three inbred backgrounds analyzed (129S2/SvPas, FVB/N, and C57BL/6J). No further organ abnormalities were detected on gross necropsy and histopathology of several organ systems, including bone histomorphometry (not shown). This is in contrast with the observations by Saleem et al., where a suggested loss-of-function allele of *Zdhhc13* results in a severe phenotype with systemic amyloidosis, osteoporosis, and premature death (Saleem *et al.*, 2010). See **Supplementary Table 1** for a comparison.

Identification of a premature stop codon in the *Zdhhc13* gene

In order to determine the genetic localization of *luc*, 375 *luc*/*luc* hybrid F2 mice were genotyped with a panel of polymorphic microsatellite markers covering the whole mouse genome. This allowed us to map *luc* in a ~1.5 Mb interval of proximal mouse chromosome 7 (~47.4 - 48.9 Mb). After sequencing several genes in the candidate region, we found that *Zdhhc13* from *luc/luc* mice contained a T to A transversion in exon 7, leading to a premature stop codon (L203X) (**Figure 2a**). The predicted termination of translation would occur after the first 200 amino acids of the *N*-terminus (**Figure 2b**), retaining only the first three ankyrin repeats. To investigate whether this nonsense mutation resulted in reduced *Zdhhc13* expression, we analyzed total brain, skin, and lung RNA by quantitative real-time PCR. We found a decreased expression of *Zdhhc13* in *luc*/*luc* mice compared with control littermates in brain, whole skin, and lung (55%, 67% and 70% reduction, respectively), indicating the presence of active nonsense-mediated mRNA decay (**Figure 2c**). We also investigated the expression pattern of *Zdhhc13* in the skin by in situ hybridization (ISH) and found that was expressed in the anagen hair follicle (HF) of WT mice at P15. However, mRNA expression was markedly reduced in mutant HFs (**Figure 2d**).

Then we compared the subcellular localization of WT and predicted mutant ZDHHC13 protein, lacking ankyrin and transmembrane domains as well as the DQHC PAT motif (ZDHHC13 contains a DQHC motif in place of the canonical DHHC). NIH3T3 cells were transiently transfected with expression vectors carrying GFP-alone, GFP-ZDHHC13-WT or GFP-ZDHHC13-truncated fusion constructs. While exogenous WT protein co-localized with a structure consistent with the Golgi apparatus (as expected), the truncated mutant ZDHHC13 showed an abnormal localization with a diffuse, homogeneous distribution in the cytoplasm and nucleus (**Figure 2e**). We confirmed these results using HeLa cells and anti RCAS1 antibodies (**Supplementary Figure S1 online**). Due to the lack of a reliable antibody against ZDHHC13, we were unable to assess protein levels or the presence of a truncated protein in mutant tissues.

To determine whether the truncated ZDHHC13 exhibited a loss-of-function for PAT activity, we assessed the skin protein palmitoylation status by using the acyl-biotin exchange assay. Only one band showed significant palmitoylation in skin samples from WT mice corresponding to MW ~80 kD. In samples from *luc*/*luc* mice, this band was decreased by >80% compared to WT, indicating that the PAT activity of ZDHHC13 was indeed abolished in mutants (**Figure 2f**).

ZDHHC13 is required for normal HF cycling and epidermal differentiation

At P1, P5, and P9, HF morphogenesis in the dorsal skin of *luc/luc* mutant mice appeared normal upon histopathological analysis; however, many HSs were twisting within the HF infundibulum and showed irregular distribution of pigment. At P15, the dorsal skin of mutant mice showed thickened epidermis with orthokeratotic hyperkeratosis. Some HSs penetrated the skin, yet some were broken, short, or twisted within the hair canal, with irregular or clumped pigment (**Figure 3a**). Analysis of HF cycle stages at P15 showed that some HFs in the mutant skin were prematurely at the early stages of regression, however this phenotype was not always present in mutant mice. Analysis of the expression of epidermal differentiation markers by immunohistochemistry (IHC) in P15 *luc*/*luc* skin showed atypical expression of K1, K5, and K6. That is, K5 was detected not only in the basal layer but also in the suprabasal layers of the epidermis, K1 was detected in all the layers while normally it is limited to the suprabasal layers, and K6 was abnormally expressed in the interfollicular epidermis (normally restricted to HF keratinocytes) (**Supplementary Figure S2 online**).

The phenotype of HF abnormality was further investigated by scanning (SEM) and transmission (TEM) electron microscopy and by IHC staining for differentiation markers expressed in the innermost layer of the outer root sheath (ORS) as well as the inner root sheath (IRS) and HS. Using TEM we found no differences in the ultrastructure of ORS, Henle's layer, Huxley's layer, cortex or medulla when comparing WT and mutant HFs (**Supplementary Figure S2 online**). The IHC analysis did not reveal any qualitative difference in the expression pattern of K16, K17, trichohyalin, or desmoglein-4 at P15 (**Supplementary Figure S3 online**). While the main morphological features of mutant HFs were abnormalities in shape and structure of HSs as well as changes in the hair cycle pace, such abnormalities were not found in those HSs that were examined by IHC and electron microscopy. Hence the pathogenesis of the alopecic phenotype in mutant mice remains obscure.

At P21, epidermal thickness was increased in mutant mice compared with WT (**Figure 3b**). The presence of epidermal hyperplasia in mutants suggested increased proliferation of keratinocytes. To verify this, we examined the expression of Ki-67, which showed an increased number of positive cells in the basal and suprabasal layers of mutant epidermis compared with WT ($p<0.03$, n=4 mice per group), confirming hyperproliferation of keratinocytes in basal conditions (**Figure 3c**). At this age, the mutant skin also displayed varying degrees of HF dysplasia and sebaceous gland (SG) hyperplasia (**Figure 3b**).

At P28 the skin phenotype became more severe, with marked epidermal and sebaceous hyperplasia. Whereas WT HFs were all in anagen VI with HSs penetrating the epidermis, HFs in mutant mice were mostly in anagen stage V, with the tip of the newly built HS still within the follicular infundibulum. Compared with littermate controls, mutant HFs were shorter and thinner, and showed fewer old club hairs (**Figure 3d**). Using SEM, we found that most of the HSs from mutants showed cuticular scales with a rough surface and irregular ill-defined cell borders (**Figure 3e**), a feature not seen in WT HSs. No differences in HF density were found in horizontal sections of dorsal skin when comparing mutant with WT skin at P7 and P28 (not shown).

At P45, the majority of the WT HFs were in telogen, while most of the HFs in mutants were in anagen, with prominent SGs and a dilated follicular infundibulum. Analysis of 6-month-old *luc*/*luc* skin showed that epidermal and SG hyperplasia and orthokeratosis were still present at this time, with HFs predominantly in anagen, features not seen in littermate controls (**Figure 3f**).

To characterize the expression of *Zdhhc13* in the epidermis we measured RNA by quantitative real-time PCR (qRT-PCR) at different time points covering part of the first postnatal HF cycle. Interestingly, the expression of *Zdhhc13* in WT epidermis, while low compared with lung and brain, seems to be linked to the HF cycle. Although not statistically significant, *Zdhhc13* mRNA levels were higher during anagen stages (P7 and P28) and lower during anagen–catagen transition (P14) and telogen (P21) (**Figure 3g**). The epidermal expression of *Zdhhc13* in *luc*/*luc* mice was decreased when compared with WT littermates (at least 60% reduction) at all the time points analyzed (not shown).

To evaluate hair regrowth, the backs of *luc*/*luc* mice and WT were imaged at 0, 4, 8, and 15 days after shaving with electric clippers. Despite some individual variation, accelerated hair regrowth was clearly evident in mutant mice when compared with WT, with some mutants showing asynchronous regrowth (**Supplementary Figure S4 online**). This is consistent with the histological observation that starting at 6-wk, mutant HFs were predominantly in anagen.

To determine the effect of ZDHHC13 deficiency on keratinocyte migration *in vitro*, we compared scratch assays with confluent keratinocyte monolayers isolated from *luc*/*luc* and WT. Keratinocytes were cultured in the presence of mitomycin C and were thus mitotically inactive. Mutant keratinocytes exhibited an augmented migratory activity and covered a greater area of the scratch compared to controls. This enhancement of the wound closure was observed at both 24 and 48 h post-scratching and was statistically significant ($p<0.05$) (**Supplementary Figure S5 online**).

Increased keratinocyte proliferation and transit in *Zdhhc13*-deficient epidermis

To evaluate the response of skin to the pro-proliferative effect of a tumor promoter, mutant and WT mice were treated topically with TPA. Following 4 treatments of 3.4 nmol TPA over a 2-wk period, the epidermis of *luc*/*luc* was strongly hyperplastic, whereas WT epidermis exhibited only a mild acanthosis. The thickness of mutant epidermis was 39.2±6.7 μm, while WT was 23.9±7.5 μm ($p<0.01$, n=6 mice per group). The number of BrdU positive nuclei in the epidermis was significantly higher in FVB/N-*luc*/*luc* mice when compared to WT ($p<0.01$, n=6 mice per group), suggesting an increase in keratinocyte proliferation in mutant skin (**Figure 4a**).

Next, we analyzed keratinocyte transit through the epidermis by following the fate of BrdU-labeled cells at 8 and 18 h after BrdU injection (17 h after the last of 4 TPA applications). The transit of keratinocytes was accelerated in *luc*/*luc* compared with WT in the two time points analyzed. Already after 8 h, many labeled keratinocytes of the mutant epidermis had reached the granular layer, whereas in WT, basal and suprabasal keratinocytes retained most of the BrdU labeled nuclei (**Figure 4b**). The number of BrdU-labeled nuclei was also

increased in non-treated skin from 6-8-wk old mutant mice when compared with WT (p<0.008, n=4 mice per group) (**Figure 4c).**

Next, we sought to assess the response of *Zdhhc13*-deficient mutant skin to acute UVB irradiation. When compared with irradiated control skin, the epidermal thickness was significantly increased in mutant skin 18 h after a single dose of UVB (2 kJ/m^2). UVB-induced keratinocyte proliferation was also greatly increased in mutants compared with WT, as measured by BrdU-positive nuclei (**Figure 4d**). In mutant skin, acanthosis was always accompanied by marked SG hyperplasia (**Figure 4d-g**), an exacerbation of the hyperplasia observed in non-irradiated skin. To determine if the lack of ZDHHC13 leads to a defective response to UV-induced DNA damage, we measured (IHC) levels of markers for DNA damage, cell-cycle arrest, and survival in mutant and WT skin sections following acute UVB irradiation. As expected, p-STAT3, p21, and p53 protein expression was elevated after acute UVB in both mutant and WT skin. However, a highly-statistically significant increase in nuclear staining for p-STAT3, p21, and p53 was seen in both basal and suprabasal keratinocytes in mutant epidermis (**Figure 4e-g**), representing abnormal proliferation in the presence of DNA damage.

Loss of ZDHHC13 leads to activation of NF-κB

NF-κB is known to play a role in keratinocyte proliferation and differentiation (Sur *et al.*, 2008). Thus, we sought to assess the possible involvement of the NF-κB pathway in the abnormal epidermal differentiation observed in *Zdhhc13*-deficient mutant mice. We first examined the expression of the p-NF-κB-p65 subunit in untreated mutant and WT skin by IHC. The analysis of untreated mutant skin showed high levels of nuclear staining for p-NF-κB in keratinocytes throughout all the epidermal layers, as well as the ORS and SGs (p<0.001, n=4 mice per group) (**Figure 5a and b**), while in WT skin the expression of p-NF-κB was lower and restricted mostly to the basal layer. Second, we examined p-NF-κB levels in mutant and WT skin following 4 TPA applications. The analysis showed increased nuclear staining for p-NF-κB 8 h after the last TPA treatment in all the layers of the epidermis and ORS in mutant skin, compared with WT (p<0.001, n=4 mice per group) (**Figure 5c**). Using Western blotting, we could confirm the activation of NF-κB as judged by the increased p52 phosphorylation in untreated mutant skin (1.6-fold of WT) (**Figure 5d**). These results are consistent with the decreased protein levels of p100, precursor of p52, in skin samples from mutant mice compared to WT (not shown).

Increased neutrophil recruitment and elastase activity in *Zdhhc13*-deficient skin

A number of studies suggest that NF-κB activation has a major role in inflammation. Thus, we assessed the inflammatory response in the skin of mutant FVB/N-*luc/luc* and WT after acute exposure to UVB and TPA. Whole mouse imaging with an enzyme-activatable fluorogenic probe was used for *in vivo* quantification of neutrophil elastase activity. We could observe that the fluorescence was greatly enhanced in mutant skin, relative to WT, both after single treatments with UVB or TPA (**Figure 5e**), suggesting increased neutrophil elastase activity in the *Zdhhc13*-deficient skin. However, mutant skin showed no differences in macrophage infiltration as measured by IHC and *in vivo* imaging with a pan-cathepsin

activatable probe. We could confirm the increase in neutrophil infiltration in H&E- and LY6G-stained dorsal skin from the same mice treated with UVB or TPA (**Figure 5f and g**).

Skin tumorigenesis is enhanced in *Zdhhc13*-deficient mice

To determine if the absence of a functional ZDHHC13 has an effect on skin tumor development, we conducted a standard two-stage skin carcinogenesis with *luc/luc* and WT littermates (FVB/N). TPA treatment was stopped after 15 wk due to excessive tumor burden in mutant mice. WTs started to develop papillomas after 6 wk of TPA treatment and reached an average of 10.3 papillomas per mouse at the end of the study (15 wk). In contrast, FVB/N-*luc*/*luc* mice developed papillomas as early as 4 wk of TPA, and the number of papillomas reached an average of 23.6 papillomas per mouse at 15 wk ($p<0.001$ vs. control mice, n=10 mice per group) (**Figure 6a and b**). By 10 wk of TPA promotion, 100% of the mice in both groups had developed papillomas. Using previously described criteria for evaluating skin tumors (Thomas-Ahner *et al.*, 2007), we determined that at 15 wk of TPA treatment mutants showed more advanced tumors than the WT, with 15.4% of the tumors classified as squamous cell carcinoma (SCC), versus only 2.4% in WT. In addition, 13.3% of the papillomas in mutant mice showed evidence of early stromal invasion, in contrast to 5.0% in WT. Based on the early invasion of SCCs in mutants, we sought to compare the expression of markers of epithelial-mesenchymal transformation (EMT). Using IHC, we found higher expression of Slug, Snail, and MMP9 and reduced levels of E-cadherin in mutant papillomas when compared with control tumors (**Figure 6c-f**), in agreement with the increased invasiveness observed in *Zdhhc13*-deficient SCC.

DISCUSSION

Post-translational palmitoylation has been shown to be involved in diverse biological processes (Zhang *et al.*, 1998; Fukata and Fukata, 2010; Mohammed *et al.*, 2013). More recently, new roles for PAT enzymes have been highlighted and their dysregulation is linked to a broad range of diseases including neurological disorders and cancer (Greaves and Chamberlain, 2011 and 2014). Several PATs, including ZDHHC2, ZDHHC9, ZDHHC11, ZDHHC14, ZDHHC17, and ZDHHC20, have been associated with tumor progression or suppression (Ducker *et al.*, 2004; Mansilla *et al.*, 2007; Zhang *et al.*, 2008; Planey *et al.*, 2009; Draper and Smith, 2010; Yeste Velasco *et al.*, 2014). There are very limited data currently available relating ZDHHC13 with cancer.

In this study we demonstrate that mice with a mutation in the *Zdhhc13* gene develop alopecia associated with epidermal hyperplasia and increased keratinocyte proliferation, basally and after short-term TPA applications or acute UVB irradiation. Furthermore, using a skin carcinogenesis protocol, we also found that tumor multiplicity was significantly higher in mutant mice compared with WT, and that papillomas from mutants showed accelerated malignant progression. ZDHHC13 and ZDHHC21 were recently reported to regulate skin homeostasis in the mouse (Mill et al., 2009; Saleem et al., 2010). Hence, the presence of alopecia in *luc*/*luc* mice supports previous evidence that ZDHHC13 is required for normal HF development and epidermal differentiation. However, a complete histopathological description of the skin phenotype on *Zdhhc13*-deficient mice was still

missing. In this study we provide a complete analysis of HF morphogenesis and cycling of *Zdhhc13*-deficient mice and show that the *Zdhhc13* gene has a dynamic pattern of expression in normal epidermis, probably linked with the HF cycle. As measured by qRT-PCR in WT skin, the *Zdhhc13* mRNA expression tends to be higher in the anagen stages (P7 and P28) of the first postnatal HF cycle. This is in agreement with previous findings by Northern blotting showing that *Zdhhc13* is expressed most highly in WT skin at P8 (Saleem *et al.*, 2010).

In addition, our studies provide the first demonstration for a protective role of ZDHHC13 in chemical-induced skin cancer in the mouse. Although the biochemical mechanism as to why the lack of functional ZDHHC13 conveys this protection remains unclear, the accelerated tumorigenesis is consistent with the general hyperproliferative and inflammatory phenotype and the increased expression of NF-κB observed in the skin of the mutant mice (Budunova *et al.*, 1999).

Concerning the skin phenotype and gross appearance, our mutant mice are reminiscent of the *Zdhhc13* knock-out developed by the laboratory of Dr. Michael Hayden (Sutton *et al.*, 2013), which supports the idea that *luc* is a loss-of-function allele of *Zdhhc13*. However, the nonsense mutation described by Saleem et al. (R425X, exon 12), induced by N-ethyl-N-nitrosourea (ENU), has a more severe phenotype, including osteoporosis-related kyphosis, systemic amyloidosis, and reduced lifespan, data that raise questions about the nature of this supposedly loss-of-function mutation (Saleem *et al.*, 2010; Song *et al.*, 2014). The striking differences in phenotype between the R425X mutants and our *luc*/*luc* mice (and the *Zdhhc13* knock-out) are very difficult to explain based solely on the genetic background, since we have analyzed four non-related backgrounds, some of which are also part of the background of the R425X mutants. One possibility is that the R425X mutation is acting in a dominant-negative manner (Sutton *et al.*, 2013), particularly knowing that the expected truncated protein retains all the ankyrin domains, sufficient for some protein interactions (Lemonidis *et al.,* 2014). The other possibility is the presence of undetected (passenger) mutations on the background of the R425X mutant line (likely induced by the ENU mutagenesis). See **Supplementary Table 1** for a comparison of all the available *Zdhhc13* mutant alleles and related phenotypes.

ZDHHC13, known largely to catalyze the palmitoylation of Huntingtin (Goytain *et al.*, 2008), has also been suggested to be involved in both NF-κB and MAPK signaling pathways (Matsuda *et al.*, 2003). Others have reported mouse models where the NF-κB pathway is altered and that exhibit phenotypes similar to our *luc/luc* mice. For example, in knock-in mice expressing a mutant p65, increased NF-κB activity leads to epidermal hyperplasia and keratinocyte hyperproliferation, and promotes the development of keratoacanthomas after DMBA/TPA (Poligone *et al.*, 2013). Similarly, the well-known susceptibility of hairless (Hr^{hr}/Hr^{hr}) mice to UVB-induced tumorigenesis was recently linked to a disruption of the NF-κB pathway. As in our *luc/luc* mice, hairless mice also show epidermal hyperplasia, basally and after UVB exposure, associated with constitutive activation of the NF-κB signaling and increased p65 levels in the epidermis (Kim *et al.*, 2012). Moreover, reduction in *Zdhhc13* mRNA expression was observed in the skin of K5-IKKb transgenic mice (RNA microarrays data from Gene Expression Omnibus). This model overexpressing IKK-β in the

basal layer of the epidermis shares with our mutants the sustained activation of NF-κB and infiltration of inflammatory cells in the dermis, a phenotype that is similarly independent of T and B cells (Page *et al.*, 2010).

The role of NF-κB in the skin is not yet completely understood (Sur *et al.*, 2008). Thus, further studies are needed to clarify which substrates, if any, in the NF-κB signaling pathway are palmitoylated by ZDHHC13. This is conceivable, since NF-κB is known to contain sites for post-translational modifications that are important for crosstalk with other pathways (Perkins, 2006; Hoesel and Schmid, 2013). Together with the constitutive expression of NF-κB after TPA and UVB, the skin from our *Zdhh13*-deficient mice showed marked neutrophilic infiltration of the dermis and increased neutrophil elastase activity. This is not surprising, as neutrophils are known to play an important role in cancer-related inflammation, including in mouse models of multistage carcinogenesis (Moore *et al.*, 1999; Nozawa *et al*., 2006; Decicco-Skinner *et al*., 2011). Likewise, neutrophil elastase (a major product of neutrophils) was associated with the development of UVB- and benzopyrene-induced skin tumors in hairless mice, where a reduction in its activity can greatly reduce the incidence of tumors (Starcher *et al.*, 1996).

In the last years, numerous somatic mutations in cancer have been revealed using whole-genome sequencing and all these data are available on line. Specifically, *Zdhhc13* was found mutated in human metastatic melanoma with a mutation frequency of approximately 4% (25 samples analyzed) (Berger *et al*, 2012). At the RNA level, *Zdhhc13* was found to be up-regulated (1.9-fold-change; Significance Analysis of Microarrays Score 5.0) in human hepatocellular carcinomas (91 samples analyzed) (Villanueva *et al.,* 2008). However, the underlying mechanisms behind the link between *Zddhc13* expression and cancer need to be elucidated. Further investigations are required to understand substrate targets and possible non-canonical activities of ZDHHC13.

MATERIALS AND METHODS

Origin of the *luca* mutation

The *luc* allele arose in *Institut Pasteur*, Paris, and was originally maintained in 129S2/SvPas. The mutant allele was later introgressed into FVB/N and C57BL/6J backgrounds by marker-assisted backcrossing. See Supplemental Information online for details.

Genetic mapping

The assignment of *luc* to chromosome 7 and further fine mapping were accomplished using two independent intercrosses. F2 mice were genotyped with genome-wide microsatellite markers under standard conditions (Benavides *et al.*, 2000). See Supplemental Information online for details.

Transient expression of *Zdhhc13* cDNA in NIH3T3 cells

The coding sequences of both the WT and mutant *Zdhhc13* genes were cloned with EGFP located in the amino-terminal portion of the proteins. NIH3T3 cells were transiently transfected with the constructs and incubated for 24 hours. Cells were fixed, blocked and

stained with DAPI for imaging with a Zeiss Observer Z1 confocal microscope. See Supplemental Information online for details.

In situ hybridization and qRT-PCR

Tissue preparation and automated *in situ* hybridization were performed by the RNA In Situ Hybridization Core at Baylor College of Medicine as previously described (Yaylaoglu *et al.,* 2005). *Zdhhc13* RNA expression was analyzed from total brain, whole skin, scraped epidermis and lung by qRT-PCR using *Zdhhc13* assay on demand (Applied Biosystems, Foster City, CA) according to the manufacture's instructions. See Supplemental Information online for details.

Western blotting

Skin samples were pulverized under liquid nitrogen and proteins extracted as previously described (Napoli *et al.,* 2013). Proteins were then transferred to a nitrocellulose membrane and incubated with the primary anti total NFκB (Cell Signaling Technologies, Danvers, MA), or phospho-NFκB (Cell Signaling Technologies). See Supplemental Information online for details.

Acyl-biotin exchange (ABE) palmitoylation assay

Assessment of palmitoylation levels was carried out in skin samples as previously described (Drisdel and Green, 2004) (Drisdel *et al.,* 2006), with some modifications. See Supplemental Information online for details.

Tissue collection, immunohistochemistry, and electron microscopy

Untreated dorsal skin, TPA- and UVB-treated dorsal skin and skin tumors from *luc*/*luc* and WT were fixed and stained with hematoxylin and eosin. IHC was performed with antibodies directed against mouse proteins as previously described (Benavides *et al.*, 2002). The electron microscope images were obtained from the High Resolution Electron Microscopy Facility (HREMF) at MD Anderson. See Supplemental Information online for details.

Analysis of cell proliferation following TPA treatment and UVB exposure

The shaved dorsal skin of FVB/N-*luc*/*luc* and WT mice was treated either with twice-weekly topical applications of TPA (4 μg/200 μl acetone) for 2 wk or a single UV treatment (2 kJ/m^2). Treated mice received BrdU prior to euthanasia. For *in vivo* keratinocyte transit studies, mice were injected with BrdU 17 h after the last of four TPA applications over a two-week period and sacrificed 8 h and 18 h after BrdU as described (Tiano *et al.,* 2002). See Supplemental Information online for details.

In vivo imaging

Two activatable-fluorescent agents were used, ProSense 750 and Neutrophil Elastase 680 (PerkinElmer, Waltham, MA). Animals were imaged using an IVIS Spectrum system. Acquired images were analyzed using LivingImage 4.4 (Caliper Life Sciences). See Supplemental Information online for details.

Chemical skin carcinogenesis and tissue collection

The two-stage carcinogenesis was performed as previously described (Benavides *et al.*, 2011). See Supplemental Information online for details.

Supplementary Material

Refer to Web version on PubMed Central for supplementary material.

ACKNOWLEDGMENTS

We thank the Research Animal Support Facility-Smithville for their assistance with the maintenance of the mouse strains, the Histology and Tissue Processing Facility Core for processing the samples, the Molecular Biology Facility Core for DNA sequencing, and Kevin Lin for statistical analyses. We also acknowledge Sarah Adai for proofreading the manuscript. This study made use of the Research Animal Support Facility-Smithville (including Genetic Services and Mutant Mouse Pathology Services), the Bone Histomorphometry Core, and the High Resolution Electron Microscopy Facility (HREMF), which are supported by P30 CA016672 DHHS/NCI Cancer Center Support Grant to MD Anderson Cancer Center. This study also made use of the RNA In Situ Hybridization Core at Baylor College of Medicine, Texas, which is, in part, supported by a Shared Instrumentation grant from the NIH (1S10OD016167). This work was supported by the Baker Foundation Pilot Project to FB; by the "Youth Excellence scholarship" from Caja de Burgos to LM, by the CHDI Foundation (A-2638 & A-4489) to CG; and by the National Institutes of Health (NIH) Grant CA132840 from the National Cancer Institute and the Grady F. Saunders, PhD Distinguished Professorship to RDW.

REFERENCES

Benavides F, Blando J, Contreras O, et al. Protective role of cathepsin L in mouse skin carcinogenesis. Mol Carcinog advance online publication. May 2.2011 DOI.

Benavides F, Starost MF, Flores M, et al. Impaired hair follicle morphogenesis and cycling with abnormal epidermal differentiation in nackt mice, a cathepsin L-deficient mutation. Am J Pathol. 2002; 161:693–703. [PubMed: 12163394]

Benavides F, Stern MC, Glasscock E, et al. Microsatellite DNA variants between the inbred SENCAR mouse strains. Mol Carcinog. 2000; 28:191–5. [PubMed: 10972988]

Berger MF, Hodis E, Heffernan TP, et al. Melanoma genome sequencing reveals frequent PREX2 mutations. Nature. 2012; 485:502–6. [PubMed: 22622578]

Budunova IV, Perez P, Vaden VR, et al. Increased expression of p50-NF-kappaB and constitutive activation of NF-kappaB transcription factors during mouse skin carcinogenesis. Oncogene. 1999; 18:7423–31. [PubMed: 10602501]

Cataisson C, Ohman R, Patel G, et al. Inducible cutaneous inflammation reveals a pro tumorigenic role for keratinocyte CXCR2 in skin carcinogenesis. Cancer Res. 2009; 69:319–28. [PubMed: 19118017]

Decicco-Skinner KL, Trovato EL, Simmons JK, et al. Loss of tumor progression locus 2 (tpl2) enhances tumorigenesis and inflammation in two-stage skin carcinogenesis. Oncogene. 2011; 30:389–97. [PubMed: 20935675]

Draper JM, Smith CD. Palmitoyl acyltransferase assays and inhibitors. Mol Membr Biol. 2009; 26:5–13. [PubMed: 19152182]

Draper JM, Smith CD. DHHC20: a human palmitoyl acyltransferase that causes cellular transformation. Mol Membr Biol. 2010; 27:123–36. [PubMed: 20334580]

Draper JM, Xia Z, Smith CD. Cellular palmitoylation and trafficking of lipidated peptides. J Lipid Res. 2007; 48:1873–84. [PubMed: 17525474]

Drisdel RC, Alexander JK, Sayeed A, et al. Assays of protein palmitoylation. Methods. 2006; 40:127–34. [PubMed: 17012024]

Drisdel RC, Green WN. Labeling and quantifying sites of protein palmitoylation. Biotechniques. 2004; 36:276–85. [PubMed: 14989092]

Ducker CE, Stettler EM, French KJ, et al. Huntingtin interacting protein 14 is an oncogenic human protein: palmitoyl acyltransferase. Oncogene. 2004; 23:9230–7. [PubMed: 15489887]

Fukata Y, Fukata M. Protein palmitoylation in neuronal development and synaptic plasticity. Nat Rev Neurosci. 2010; 11:161–75. [PubMed: 20168314]

Fukata Y, Iwanaga T, Fukata M. Systematic screening for palmitoyl transferase activity of the DHHC protein family in mammalian cells. Methods. 2006; 40:177–82. [PubMed: 17012030]

Goytain A, Hines RM, Quamme GA. Huntingtin-interacting proteins, HIP14 and HIP14L, mediate dual functions, palmitoyl acyltransferase and Mg2+ transport. J Biol Chem. 2008; 283:33365–74. [PubMed: 18794299]

Greaves J, Chamberlain LH. DHHC palmitoyl transferases: substrate interactions and (patho)physiology. Trends Biochem Sci. 2011; 36:245–53. [PubMed: 21388813]

Greaves J, Chamberlain LH. New links between S-acylation and cancer. J Pathol. 2014; 233:4–6. [PubMed: 24615251]

Hoesel B, Schmid JA. The complexity of NF-kappaB signaling in inflammation and cancer. Mol Cancer. 2013; 12:86. [PubMed: 23915189]

Kim H, Casta A, Tang X, et al. Loss of hairless confers susceptibility to UVB-induced tumorigenesis via disruption of NF-kappaB signaling. PLoS One. 2012; 7:e39691. [PubMed: 22761871]

Lemonidis K, Gorleku OA, Sanchez-Perez MC, et al. The Golgi S-acylation machinery comprises zDHHC enzymes with major differences in substrate affinity and S acylation activity. Mol Biol Cell. 2014; 25:3870–83. [PubMed: 25253725]

Levental I, Lingwood D, Grzybek M, et al. Palmitoylation regulates raft affinity for the majority of integral raft proteins. Proc Natl Acad Sci USA. 2010; 107:22050–4. [PubMed: 21131568]

Linder ME, Deschenes RJ. Palmitoylation: policing protein stability and traffic. Nat Rev Mol Cell Biol. 2007; 8:74–84. [PubMed: 17183362]

Mansilla F, Birkenkamp-Demtroder K, Kruhoffer M, et al. Differential expression of DHHC9 in microsatellite stable and instable human colorectal cancer subgroups. Br J Cancer. 2007; 96:1896–903. [PubMed: 17519897]

Matsuda A, Suzuki Y, Honda G, et al. Large-scale identification and characterization of human genes that activate NF-kappaB and MAPK signaling pathways. Oncogene. 2003; 22:3307–18. [PubMed: 12761501]

Mill P, Lee AW, Fukata Y, et al. Palmitoylation regulates epidermal homeostasis and hair follicle differentiation. PLoS Genet. 2009; 5:e1000748. [PubMed: 19956733]

Mitchell DA, Vasudevan A, Linder ME, et al. Protein palmitoylation by a family of DHHC protein S-acyltransferases. J Lipid Res. 2006; 47:1118–27. [PubMed: 16582420]

Mohammed AM, Chen F, Kowluru A. The two faces of protein palmitoylation in islet beta-cell function: potential implications in the pathophysiology of islet metabolic dysregulation and diabetes. Recent Pat Endocr Metab Immune Drug Discov. 2013; 7:203–12. [PubMed: 23829395]

Moore RJ, Owens DM, Stamp G, et al. Mice deficient in tumor necrosis factor alpha are resistant to skin carcinogenesis. Nat Med. 1999; 5:828–31. [PubMed: 10395330]

Napoli E, Wong S, Hung C, et al. Defective mitochondrial disulfide relay system, altered mitochondrial morphology and function in Huntington's disease. Hum Mol Genet. 2013; 22:989–1004. [PubMed: 23197653]

Nozawa H, Chiu C, Hanahan D. Infiltrating neutrophils mediate the initial angiogenic switch in a mouse model of multistage carcinogenesis. Proc Natl Acad Sci USA. 2006; 103:12493–8. [PubMed: 16891410]

Page A, Navarro M, Garín M, et al. IKKbeta leads to an inflammatory skin disease resembling interface dermatitis. J Invest Dermatol. 2010; 130:1598–610. [PubMed: 20200541]

Perkins ND. Post-translational modifications regulating the activity and function of the nuclear factor kappa B pathway. Oncogene. 2006; 25:6717–30. [PubMed: 17072324]

Planey SL, Keay SK, Zhang CO, et al. Palmitoylation of cytoskeleton associated protein 4 by DHHC2 regulates antiproliferative factor-mediated signaling. Mol Biol Cell. 2009; 20:1454–63. [PubMed: 19144824]

Planey SL, Zacharias DA. Palmitoyl acyltransferases, their substrates, and novel assays to connect them. Mol Membr Biol. 2009; 26:14–31. [PubMed: 19191172]

Poligone B, Hayden MS, Chen L, et al. A role for NF-kappaB activity in skin hyperplasia and the development of Keratoacanthomata in mice. PLoS One. 2013; 8:e71887. [PubMed: 23977171]

Saleem AN, Chen YH, Baek HJ, et al. Mice with alopecia, osteoporosis, and systemic amyloidosis due to mutation in Zdhhc13, a gene coding for palmitoyl acyltransferase. PLoS Genet. 2010; 6:e1000985. [PubMed: 20548961]

Schneider CA, Rasband WS, Eliceiri KW. NIH Image to ImageJ: 25 years of image analysis. Nat Methods. 2012; 9:671–5. [PubMed: 22930834]

Song IW, Li WR, Chen LY, et al. Palmitoyl acyltransferase, zdhhc13, facilitates bone mass acquisition by regulating postnatal epiphyseal development and endochondral ossification: a mouse model. PLoS One. 2014; 9:e92194. [PubMed: 24637783]

Starcher B, O'Neal P, Granstein, et al. Inhibition of neutrophil elastase suppresses the development of skin tumors in hairless mice. J Invest Dermatol. 1996; 107:159–63. [PubMed: 8757756]

Sur I, Ulvmar M, Toftgard R. The two-faced NF kappaB in the skin. Int Rev Immunol. 2008; 27:205–23. [PubMed: 18574737]

Sutton LM, Sanders SS, Butland SL, et al. Hip14l-deficient mice develop neuropathological and behavioural features of Huntington disease. Hum Mol Genet. 2013; 22:452–65. [PubMed: 23077216]

Thomas Ahner JM, Wulff BC, Tober KL, et al. Gender differences in UVB-induced skin carcinogenesis, inflammation, and DNA damage. Cancer Res. 2007; 67:3468–74. [PubMed: 17389759]

Tiano HF, Loftin CD, Akunda J, et al. Deficiency of either cyclooxygenase (COX)-1 or COX-2 alters epidermal differentiation and reduces mouse skin tumorigenesis. Cancer Res. 2002; 62:3395–401. [PubMed: 12067981]

Villanueva A, Chiang DY, Newell P, et al. Pivotal role of mTOR signaling in hepatocellular carcinoma. Gastroenterology. 2008; 135:1972–83. [PubMed: 18929564]

Yaylaoglu MB, Titmus A, Visel A, et al. Comprehensive expression atlas of fibroblast growth factors and their receptors generated by a novel robotic in situ hybridization platform. Dev Dyn. 2005; 234:371–86. [PubMed: 16123981]

Yeste-Velasco M, Mao X, Grose R, et al. Identification of ZDHHC14 as a novel human tumour suppressor gene. J Pathol. 2014; 232:566–77. [PubMed: 24407904]

Zhang J, Planey SL, Ceballos C, et al. Identification of CKAP4/p63 as a major substrate of the palmitoyl acyltransferase DHHC2, a putative tumor suppressor, using a novel proteomics method. Mol Cell Proteomics. 2008; 7:1378–88. [PubMed: 18296695]

Zhang W, Trible RP, Samelson LE. LAT palmitoylation: its essential role in membrane microdomain targeting and tyrosine phosphorylation during T cell activation. Immunity. 1998; 9:239–46. [PubMed: 9729044]

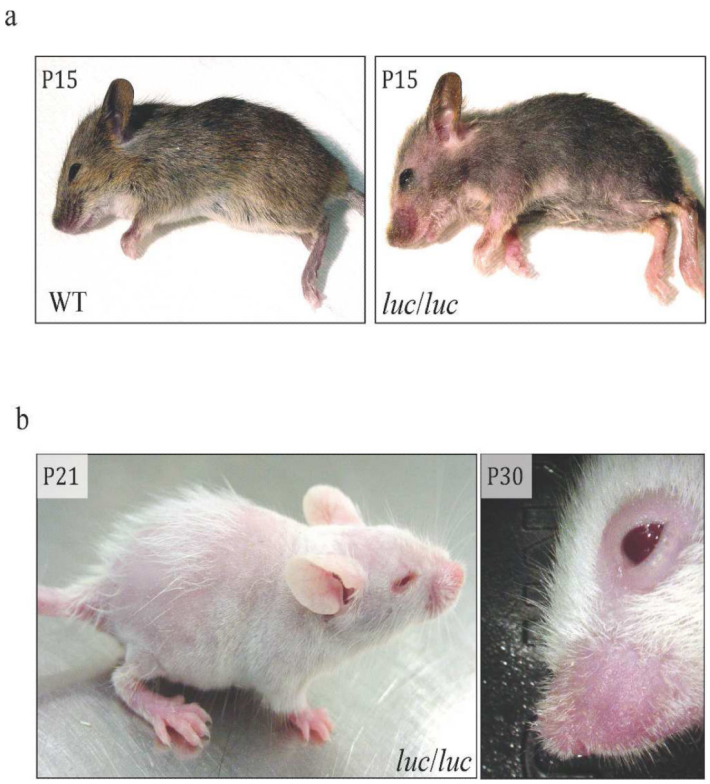

Figure 1. Skin phenotype in *Zdhhc13*-deficient *luc*/*luc* mice

(**a**) Sparse hair coat, erythema of the muzzle, and redness of the skin in a 129S2/SvPas-*luc/luc* mouse at P15 (right). Control littermate is shown on the left. (**b**) P21 FVB/N-*luc*/*luc* mouse (left) showing typical generalized alopecia at this stage. P30 FVB/N-*luc*/*luc* mouse (right) with characteristic multifocal patchy alopecia affecting the face (particularly in the periocular region) and short vibrissae. In mice older than 12 months, multifocal alopecia and erythema were associated with inflammatory cell infiltrations in the upper follicular lumen (not shown). WT, wild-type.

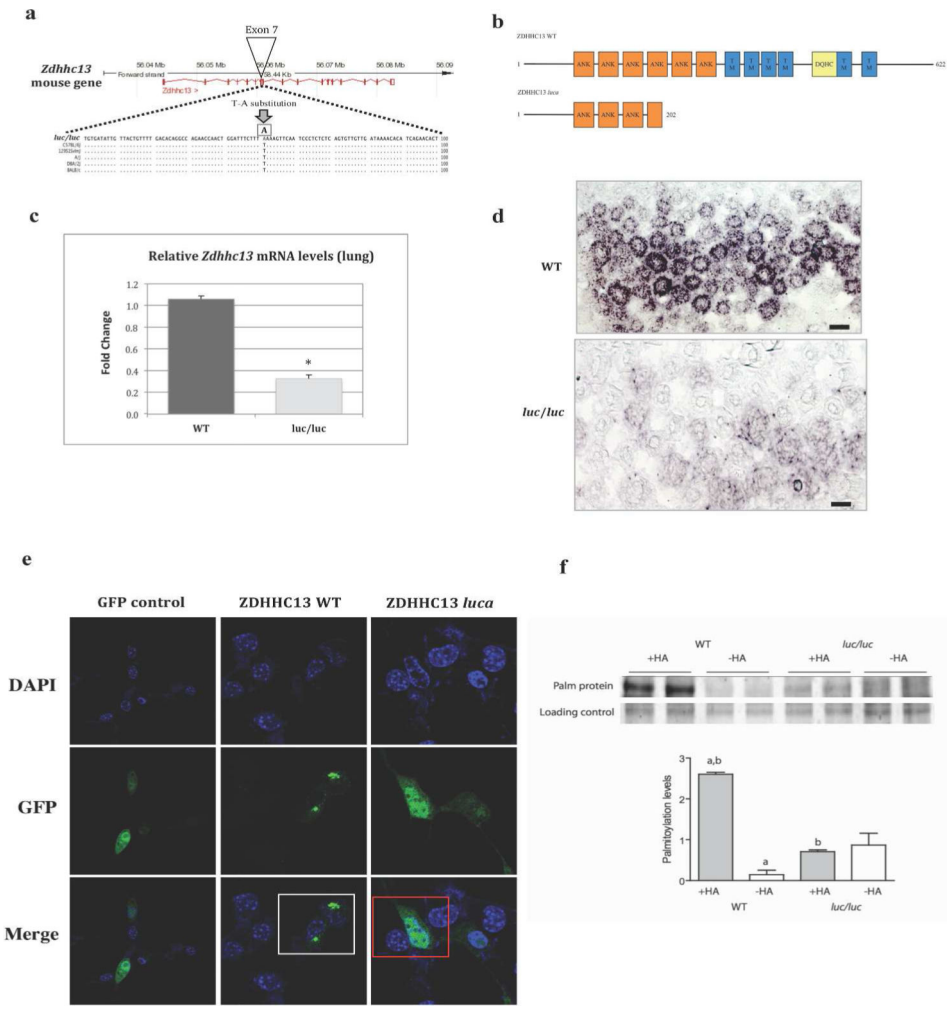

Figure 2. The *luca* mutation corresponds to a premature stop codon in the *Zdhhc13* gene

(**a**) The T to A transversion found in exon 7 of the mutant gene generates a premature stop codon (TAA replacing TTA) and a predicted truncated protein. (**b**) Diagram comparing WT ZDHHC13 with the predicted truncated protein from the mutant allele, lacking 3 out of 6 ankyrin (ANK) repeats, all transmembrane (TM) domains, and the DQHC PAT motif. (**c**) The graph shows the mean values of fold-change for *Zdhhc13* mRNA levels in WT relative to mutant lung. Control and mutant values are relative to those of internal control β-actin. Bar graph values represent mean ± SEM (*p<0.008, one-tailed unpaired Student's *t*-test). (**d**) Representative images of *in situ* hybridization in WT and mutant skin (P15). The transverse sections of the anagen HFs show a highly reduced hybridization signal for *Zdhhc13* mRNA in mutant skin relative to WT. (**e**) Localization of ZDHHC13 protein in NIH3T3 cells. While GFP-ZDHHC13-WT protein (green) localizes at the Golgi apparatus (white box), mutant GFP-ZDHHC13-truncated protein is localized throughout the cytoplasm and nucleus (red box). (**f**) Protein palmitoylation in WT and mutant skin. Data are shown as mean ± SEM (a,b: significant with *p*-value <0.01). Bars = 100 μm (d). DAPI, 4',6-Diamidino-2-phenylindole; GFP, green fluorescent protein; HA, hydroxylamine; HF, hair follicle; WT, wild type.

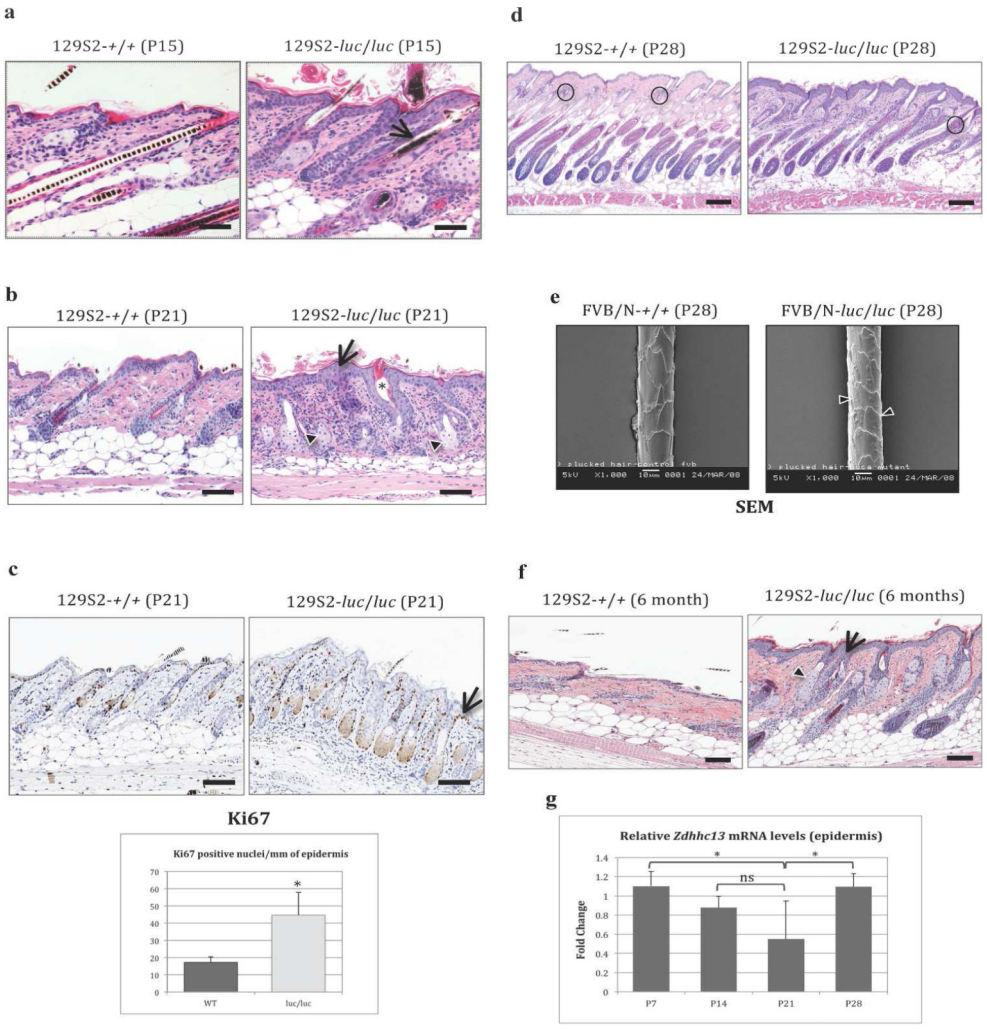

Figure 3. Histology of the 129S2/SvPas-*Zdhhc13*^{luc}/*Zdhhc13*^{luc} mutant skin

(**a**) H&E-stained dorsal skin sections from untreated WT and mutant at P15. Mutant skin shows mild epidermal hyperplasia with hyperkeratosis. Arrow shows pigment clumps in a mutant. (**b**) H&E-stained skin sections from WT and mutant at P21. Mutant skin shows markedly thickened epidermis (arrow) with orthokeratotic hyperkeratosis, HF dysplasia, and SG hyperplasia. Arrowheads show SG hyperplasia. Asterisk indicates dilated infundibulum. (**c**) Ki67-stained sections from WT and mutant at P21. Mutant skin exhibits increased number of positive nuclei in the basal and suprabasal layers of the epidermis (arrow). The bar graph represents the mean value ± SD, n=4 (*p<0.03, independent two samples t-test). (**d**) H&E sections at P28 showing anagen-stage HFs. Mutant skin shows slight delay in HF cycling, fewer old club hairs (circles), and epidermal and SG hyperplasia. (**e**) SEM image of WT HS (left) demonstrating normal arrangement of distally-oriented overlapping cuticular scales. Right, mutant HS demonstrating abnormal cuticular scales with rough surface and ill-defined borders (arrowheads). (**f**) Mutant skin at 6 months showing pronounced epidermal (arrow) and SG hyperplasia (arrowhead). (**g**) The graph shows the mean values of fold-change for *Zdhhc13* mRNA levels in WT epidermis at P7, P14, P21, and P28. Control values are relative to those of internal control (mouse GAPDH). Bar graph values represent

mean ± SEM (*p<0.08, ns: no significance, one tailed unpaired Student's *t*-test). Bars = 40 μm (a) and 100 μm (b, d and f). SEM bar = 10 μm (e). H&E, hematoxylin and eosin; HF, hair follicle; HS, hair shaft; WT, wild-type.

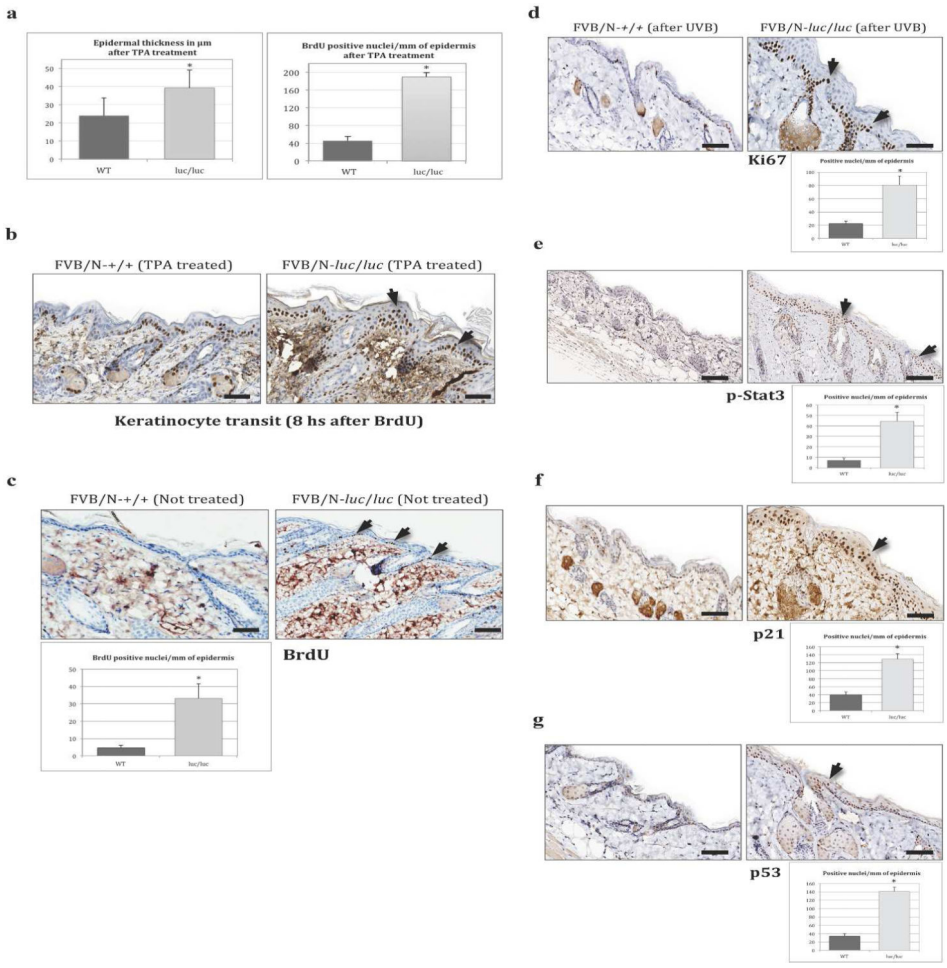

Figure 4. Increased keratinocyte proliferation and transit in mutant epidermis after acute TPA and UVB exposure

(**a**) Bar graphs show epidermal thickness in µm (left) and cell proliferation level as BrdU-positive nuclei per mm of epidermis (right) after TPA. Values represent mean ± SD (*p<0.01 both graphs). (**b**) Representative BrdU-immunostaining of TPA-treated dorsal skin from WT and mutant after 8 h of BrdU. Progression of BrdU-labeled keratinocytes towards the surface is faster in mutant epidermis (arrows show positively stained nuclei in granular layer of mutant skin, not seen in WT). (**c**) Representative BrdU-immunostaining of untreated dorsal skin from WT and mutant after BrdU (arrows show increased number of positive nuclei in the basal layer of mutant epidermis). Bar graph represents the mean value ± SD, n=4 (*p<0.008, independent two-samples t-test). (**d-g**) Representative IHC images showing localization of Ki67-, p-STAT3-, p21-, and p53-positive keratinocytes in UVB-exposed skin from WT and mutant. Arrows indicate strong positively stained nuclei in all layers of the epidermis in mutant skin, not seen in WT. Bar graphs represent mean value ± SD, n=4 (*p<0.003 for Ki67 and p-STAT3; *p<0.001 for p21 and p53, independent two-samples t-test). Bars = 40 µm (b, d, f and g) and 100 µm (c and e). BrdU, 5-bromo-2-deoxyuridine; IHC, immunohistochemistry; SD, standard deviation; TPA, 12-O-tetradecanoylphorbol-13-acetate; WT, wild-type.

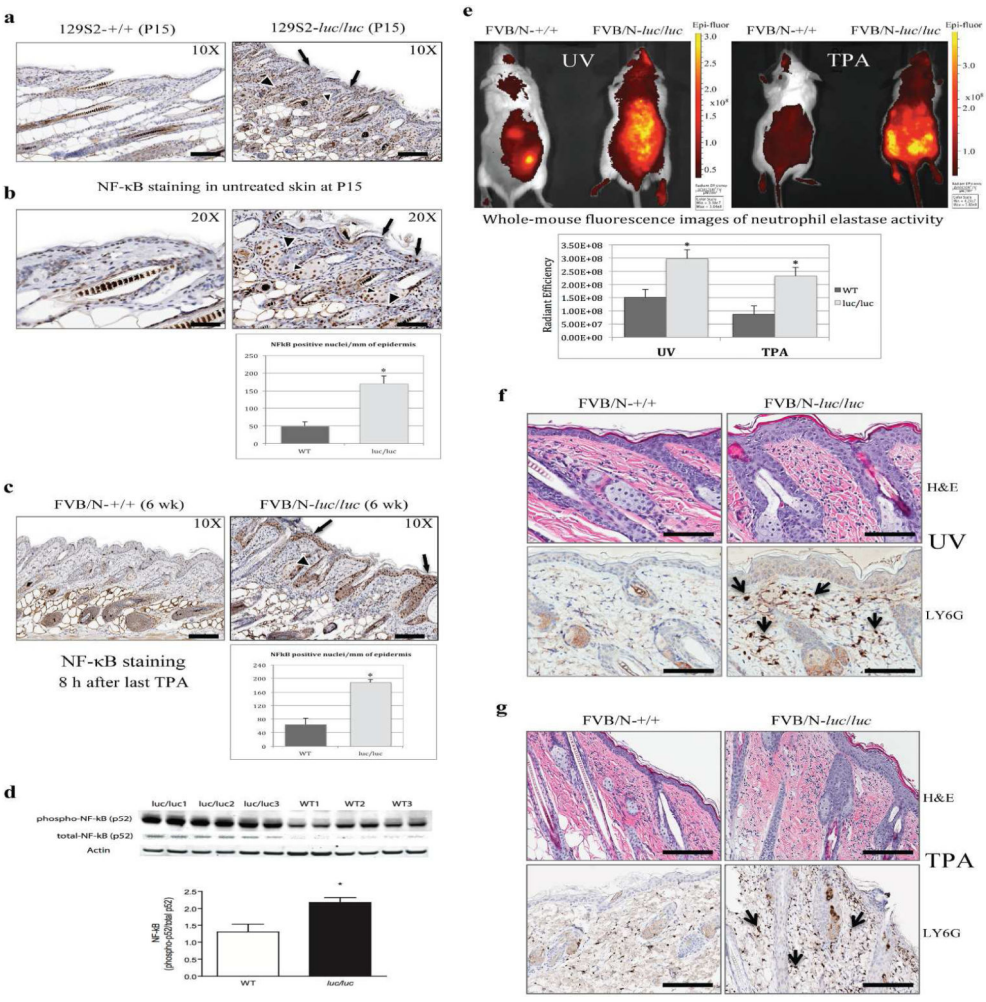

Figure 5. Constitutive activation of NF-κB and increased neutrophil recruitment in the mutant skin

(**a, b**) Representative IHC showing NF-κB expression in untreated dorsal skin. Strong positively stained nuclei (over-phosphorylated p65) are present in all layers of mutant epidermis (arrows), ORS (big arrowheads), and SGs (small arrowheads), not seen in WT. Bar graph: mean value ± SD, n=4 (*p<0.001, independent two-samples t-test). (**c**) Over-phosphorylation of p65 in mutant skin after 4 TPA treatments. Arrows show positively-stained keratinocytes on the granular layer of mutant skin 8 h after last TPA. Arrowheads indicate positively-stained nuclei in ORS. Bar graph: mean value ± SD, n=4 (*p<0.001, independent two samples t-test). (**d**) WB from total and phospho(Ser^{536})-NF-κB protein levels in untreated skin. Mean ± SEM, n=3 (*p<0.01, Student's t-test). (**e**) Whole-mouse fluorescence images of neutrophil elastase activity after UV and TPA. Color scale indicates radiant efficiency. Quantitative analysis of fluorescence levels with mutant mice showing significantly stronger signal than WT (UV-*p<0.007; TPA-*p<0.001, n=4). (**f**) H&E- and LY6G-stained sections from UVB-treated skin. Mutant skin shows markedly thickened epidermis, increased inflammatory infiltration and higher levels of LY6G-positive cells (neutrophils) in the dermis (arrows). (**g**) Similar results as in (f) in TPA-treated skin. Bars =

100 μm (a, c) and 40 μm (b, f, g). WT, wild-type; TPA, 12-O-tetradecanoylphorbol-13-acetate; H&E, hematoxylin and eosin.

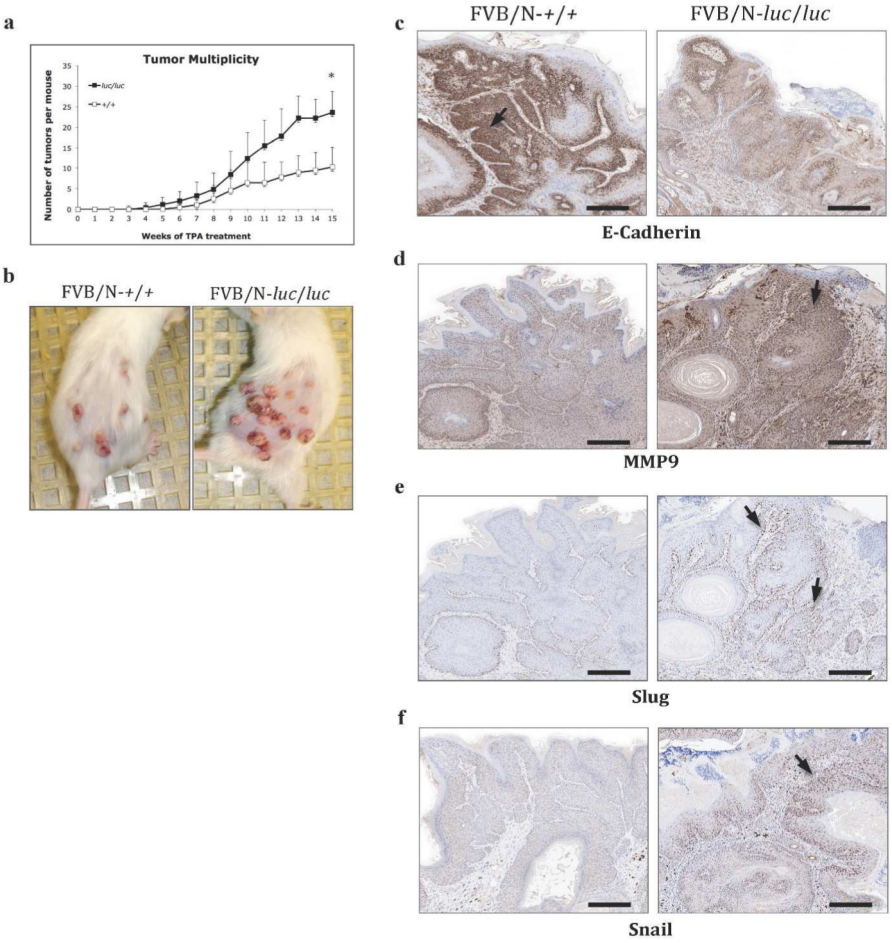

Figure 6. Increased susceptibility to skin carcinogenesis in *Zdhhc13*^{luc}/*Zdhhc13*^{luc} mutant mice

(**a**) Multiplicity of skin tumors after two stage carcinogenesis in FVB/N-*luc*/*luc* mice (n = 10) was highly statistically significant compared to that of WT littermates (n = 10) at 15 wk of TPA treatment (*p<0.001, Wilcoxon Rank Sum test). The number of papillomas was determined weekly. Tumor multiplicity is the average number of skin tumors per mouse. (**b**) Representative images of DMBA/TPA-induced skin tumors after 15 wk of TPA in WT (left) and mutant (right) FVB/N mice. (**c-f**) Representative IHC staining for E-cadherin, MMP9, Slug, and Snail in DMBA/TPA induced skin papillomas from WT and mutant mice. The papillomas from mutant mice show reduced levels of E-cadherin and higher expression of Slug, Snail, and MMP9 when compared with WT (arrows). This is in agreement with the increased invasiveness observed in mutant tumors. Bar = 200 μm. WT, wild type; wk, weeks; TPA, 12-O-tetradecanoylphorbol-13-acetate; DMBA, 7, 12-dimethylbenz [a] anthracene.